Engineering Fracture Mechanics 323 (2025) 111198

Contents lists available at ScienceDirect

Engineering Fracture Mechanics

journal homepage: www.elsevier.com/locate/engfracmech

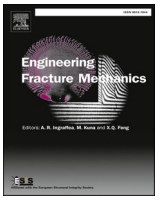

An Experimental Investigation into Fracture Resistance of Carbon Fibre Sheet Moulding Compound

Xiaodong Xu [a,*], Darren Kong Kiat Lo [b], Ilham Akbar Adi Satriya [a], Liyi Zheng [b]

[a] Centre for Aeronautics, Faculty of Engineering and Applied Sciences, Cranfield University, Cranfield MK43 0AL, UK
[b] University of Bristol, Tyndalls Park Road, Bristol BS8 1PQ, UK

ARTICLE INFO

Keywords:
Discontinuous reinforcement
Fracture toughness
R-curve
Moulding compound

ABSTRACT

Carbon Fibre Sheet Moulding Compound (CF-SMC) is an attractive material due to its good formability and green credentials. However, there is a lack of reliable fracture data, posing challenges when analysing CF-SMC materials which already have built-in randomness. Fracture Resistance curves (R-curves) and their variability have not been reported before for CF-SMC materials. This knowledge gap in the literature is addressed through Double Cantilever Beam (DCB) and first End Loaded Split (ELS) tests on CF-SMC. This work also explains the toughening mechanisms in CF-SMC materials during interlaminar fracture. Under Mode I, the toughening mechanism is fibre bridging while it is crack migration for Mode II. The new R-curve data provides new insights into the interlaminar fracture behaviour of CF-SMC materials and can be used as invaluable inputs for their failure analyses.

1. Introduction

The development of composite materials during the past half-century has had a significant impact on several industries. A composite material is the combination of various separate components to form a new material with improved qualities [1]. One of the most widely used composite materials is Carbon Fibre Reinforced Polymer (CFRP), which is expected to see continued growth in usage from 2019 to 2032 [2]. The application of CFRP in mass-produced automotive bodies has been extensively embraced, especially in vehicles from manufacturers like BMW and Audi [3]. Nonetheless, the application of CFRP presents challenges, particularly with environmental waste issues. Consequently, supporting the Sustainable Development Goals (SDGs) programme involves utilising recyclable or previously underutilised CFRP materials [4]. CFRP materials that are recyclable, or reusable can be processed and remanufactured into new products for other applications often in the form of short-fibre reinformed composites. The recycled or reused composite materials can undergo several processes to yield alternative derivative products which facilitate the utilisation of lower mechanical properties [5]. Among these composite materials, Carbon Fibre Sheet Moulding Compound (CF-SMC) is one promising option, which is commonly used in the automobile industry and for secondary components within the aerospace industry [6].

The continuous fibre composites provide remarkable strength, rigidity, and lightweight characteristics, making them highly suitable for structural applications. Moreover, its resilience to thermal and chemical stress enhances durability [6]. Through carefully tailored the surface properties e.g. wettability, roughness, and chemical functionality [7] and improved fracture performance e.g. in nano-reinforced scarf repairs [8] the continuous fibre composites can be tough too. Due to its rigidity during forming, long-fibre

* Corresponding author.
E-mail address: xiaodong.xu@cranfield.ac.uk (X. Xu).

https://doi.org/10.1016/j.engfracmech.2025.111198
Received 11 January 2025; Received in revised form 18 April 2025; Accepted 28 April 2025
Available online 1 May 2025
0013-7944/© 2025 The Author(s). Published by Elsevier Ltd. This is an open access article under the CC BY license (http://creativecommons.org/licenses/by/4.0/).

Nomenclature

Symbol	Definition
CFRP	Carbon Fibre Reinforced Polymer
SDGs	Sustainable Development Goals
CF-SMC	Carbon Fibre Sheet Moulding Compound
DCB	Double Cantilever Beam
ENF	End Notched Flexure
ELS	End Loaded Split
R-curve	Fracture resistance curve
G_{IC}	Mode I interlaminar fracture energy
P	Load
δ	Displacement
b	Specimen width
a	Measured crack length
Δ	Correction factor to account for rotation of DCB arms
F	Large displacement correction factor
C	Specimen compliance
t	Distance from centre of hinge pin to centreline of top DCB arm
L	ELS specimen free length, measured from load-line to start of clamp
h	Thickness of specimen as labelled
a_0	Film insert length
a_p	Pre-crack length
E_1	Flexural modulus determined from the clamp calibration test
Δ_{clamp}	ELS clamp correction factor
a_e	Effective crack length
G_{IIC}	Mode II interlaminar fracture energy

composites are difficult to regulate when making complex components. Short discontinuous fibre composites can be used to build complex parts but often lack strength. Common injection moulding produces lower-performance components due to discontinuous fibres, low fibre volume fraction, and orientation deviations. Long discontinuous fibre composites work well. For example, CF-SMC can mould complex components with a fibre volume fraction of 50–60 % [9], promising a potential alternative to continuous fibre composites.

Material property data is essential for accurately determining the characteristics of CF-SMC materials. Research into the fracture properties of CF-SMC is both important and appealing, which supports the material's widespread and reliable application. Methods for obtaining material property data are essential for ensuring the accuracy and validity of analytical calculations [10]. Standard test methods are available for the characterisation of interlaminar fracture toughness, such as Double Cantilever Beam (DCB) tests, End Notched Flexure (ENF) tests [11] and End Loaded Split (ELS) tests. The existing research either used assumed fracture toughness values for typical interface [12,13] or measured values using unidirectional laminates [14].

To the authors' best knowledge, there have been no reports of fracture Resistance curves (R curves) for CF-SMC materials in the literature. Few studies involved DCB and ENF tests of CF-SMC specimens. The existing paper [15] only reported a single fracture energy value from each test and stated a crack stopping behaviour without providing any detailed explanation or evidence. This study addresses the knowledge gap in the literature by experimentally quantifying R-curves of CF-SMC materials using DCB and first ELS tests. This work provides explanations for the observed Mode I and II fracture resistance behaviour in detail. The new R-curve data has significant implications for failure analyses of CF-SMC materials such as material modelling.

2. Methodology

2.1. Material and manufacturing

The material used is Hexcel's HexMC C/2000/M77-RA as shown in Fig. 1. These HexMC sheets (Fig. 1a) are made of randomly oriented prepreg tapes (Fig. 1b). During manufacturing, two HexMC raw material sheets were stacked together as illustrated in Fig. 1c. A thin layer of PTFE film (12 μm) was then placed in the middle of two double sheets to form an edge-cracked stack. The HexMC stack was cured in the autoclave at 130° C and 5 bars following the Hexcel's specification for M77 resin, for 1 hour to ensure that the target temperature was met in the composite. A hot press was not used because the existing press cannot produce a large enough plate. The cured plate was cut into five 25 × 160 mm Double Cantilever Beam (DCB) specimens according to ASTM D5528 standard [16] and four 25 × 200 mm End Loaded Split (ELS) tests according to ISO 15114 standard [17]. Piano hinges were bonded to the cracked end of the specimens (Fig. 1d) using Huntsman's Araldite 2014 two-part paste adhesive which was cured in an oven at 80° C for 1 hour.

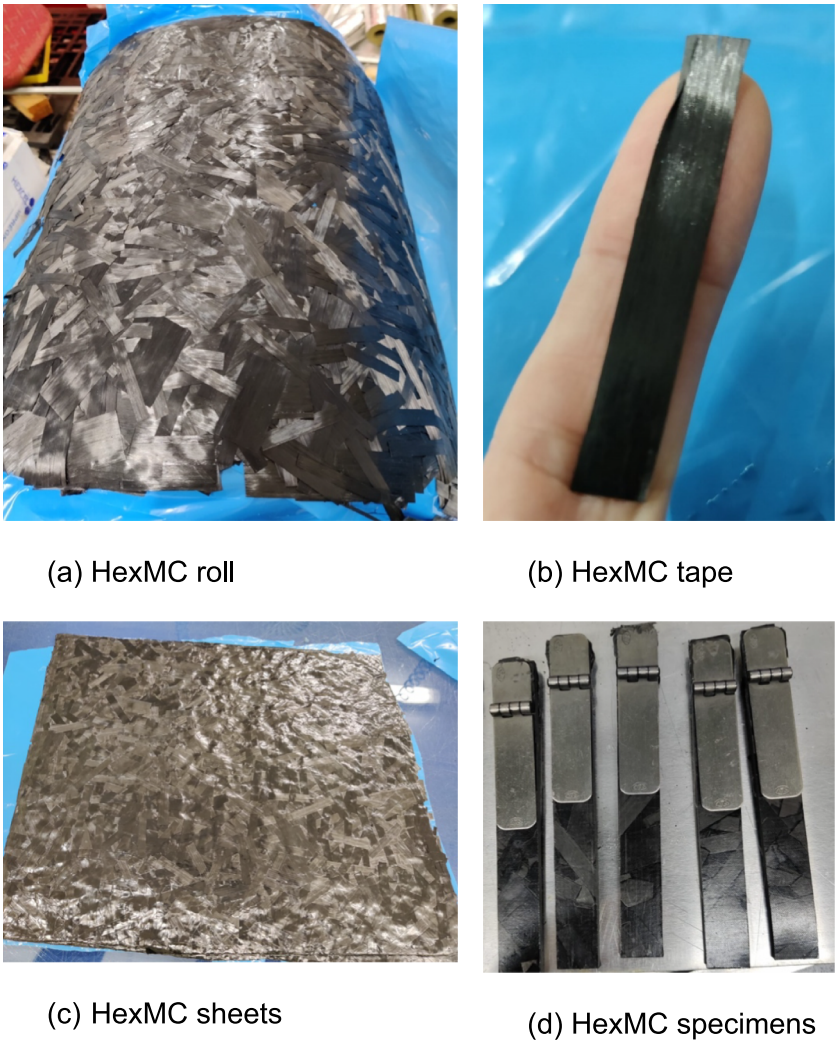

Fig. 1. HexMC raw material and cured specimens.

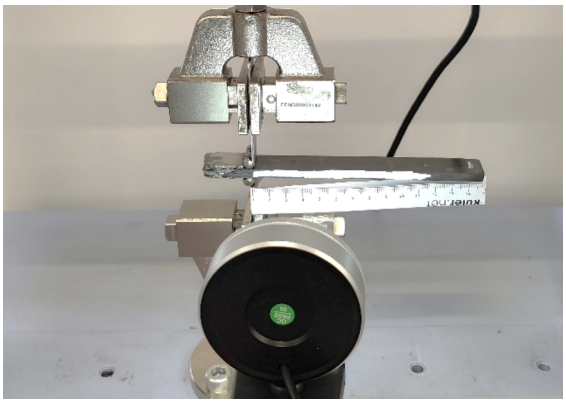

Fig. 2. DCB specimen in grips in front of a camera.

2.2. Double Cantilever Beam (DCB) test set-up

The standard test method used for Mode I interlaminar fracture is ASTM D5528 [16]. Although the standard is widely used with unidirectional laminates, it is also applicable to nonunidirectional laminates and other architectures, such as CF-SMC [15]. Following the ASTM D5528 standard, the test set-up is shown in Fig. 2.

The load was then applied by moving the upper grip upwards under displacement control at a rate of 1 mm/min, with the corresponding load–displacement data being saved. A paper ruler was attached for crack measurements (Fig. 3) using a video camera that is synchronised to start with each test. The DCB specimens were not pre-cracked.

The crack length was then matched to the recorded load and displacement at that exact times-stamp in order to be used in Mode I fracture energy, G_{IC}, calculations as per the ASTM D5528 standard. The calculation method used is the modified beam theory method as shown in Equation (1).

$$G_{\mathrm{IC}} = \frac{3P\delta}{2b(a+|\Delta|)}F \tag{1}$$

Where P, δ, b, a and Δ represents load, displacement, specimen width, crack length and the correction factor, respectively. The correction factor, Δ, is determined for individual specimens experimentally from a plot of the cube root of compliance, $\sqrt[3]{C}$, against the measured crack length. F is an additional factor to account for the shortening of the arm as well as tilting of the piano hinge and is defined in Equation (2).

$$F = 1 - \frac{3}{10}\left(\frac{\delta}{a}\right)^2 - \frac{3}{2}\left(\frac{\delta t}{a^2}\right) \tag{2}$$

Where t is the distance from the centre of hinge pin to the centreline of the top specimen arm, as can be seen in Fig. 4.

2.3. End Loaded Split (ELS) test set-up

The standard used for Mode II interlaminar fracture test is the ISO 15114 standard [17]. Fig. 5 shows the set-up and specimen design for ELS tests. The four screws in the ELS jig are tightened with an electric screwdriver to ensure consistent clamping force.

L and h are the free length and specimen half thickness respectively. a_0, a_p *and* a are the film insert length, pre-crack length and measured crack length during the test, respectively.

According to the ISO 15114 standard [17], there is a need to perform a calibration of the ELS fixture. During calibration, a specimen is set up with the crack fully within the clamped area to the right of Fig. 6. This was done to each ELS specimen to address the large specimen variability.

At a given free length, the specimen was loaded under displacement control at a rate of 1 mm/min until the force recorded reaches a 100 N and the specimen was unloaded afterwards. The specimen was then set at another free length. Six different free lengths were tested, from 50 mm to 100 mm in intervals of 10 mm. The load–displacement data was saved for each free length.

For each free length, compliance is calculated from the load–displacement data and a graph of $\sqrt[3]{C}$ against free length is plotted as shown in Fig. 7. The slope of the line is used to determine flexural modulus, E_1, according to Equation (3). The absolute value of the intercept on the free length axis is the clamp correction, Δ_{clamp}. The free length axis intercept value should be a negative value on the axis, with a positive intercept indicating errors in either data or the procedure performed.

$$E_1 = \frac{1}{2b(h \times slope)^3} \tag{3}$$

Where b is the specimen width, h is the specimen half thickness, and the slope of the trendline can also be determined from Fig. 7. h is the average value measured at three points along each ELS specimen.

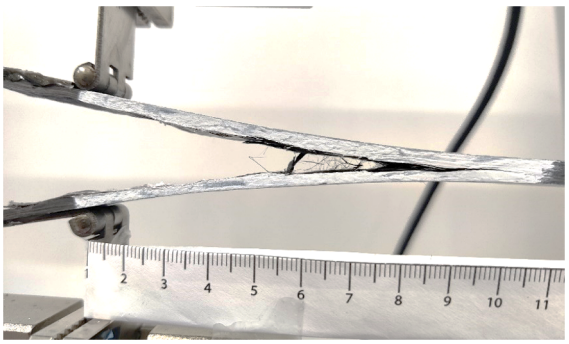

Fig. 3. Crack measurements during a DCB test.

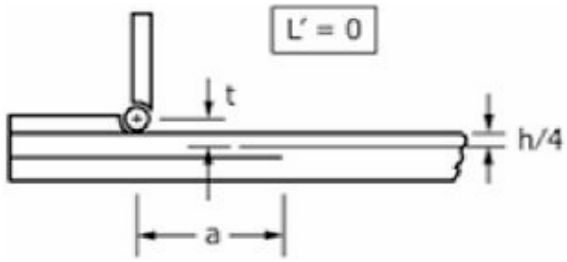

Fig. 4. F correction dimensions [16].

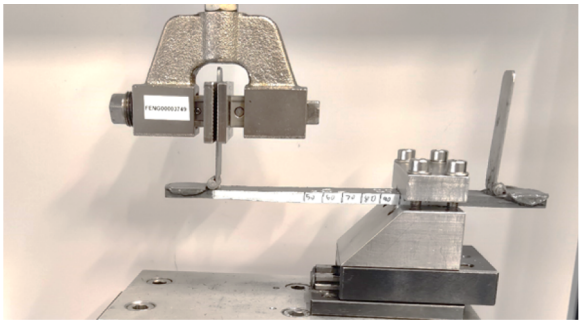

(a) ELS test set-up including a black movable platform

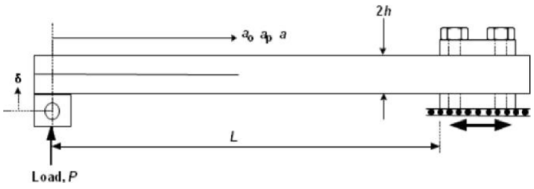

(b) ELS test schematic with labels [17]

Fig. 5. ELS specimen configuration.

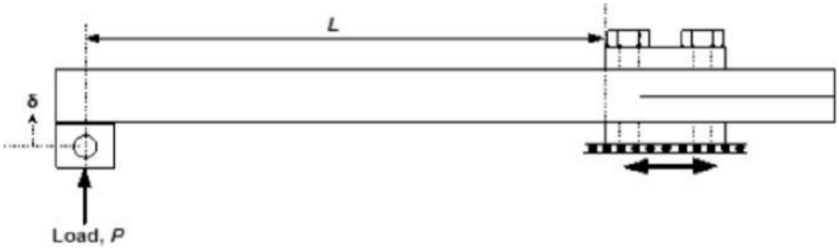

Fig. 6. ELS fixture calibration configuration [17].

Prior to the main series of static tests, the ELS specimens were pre-cracked following the ISO 15114 standard [17]. The specimens were clamped as seen in Fig. 4, with the free length L being $L = a_0/0.75$. The specimens were loaded by moving the upper grip downwards under displacement control at a rate of 1 mm/min. Loading was stopped when the crack length has grown at least 2 mm. The specimen was then unloaded.

After the pre-cracking procedure, the specimens were clamped with a different free length $L = a_p/0.55$. The specimens were loaded under displacement control at a rate of 0.5 mm/min and the tests were stopped just before the crack reached the clamp in the jig.

Following the ISO 15114 standard [17], the calculation method used is the corrected beam theory with an effective crack length approach. This approach uses compliance, C, to determine the effective crack length, a_e, so real-time crack measurement is not required. The effective crack length is calculated using Equation (4).

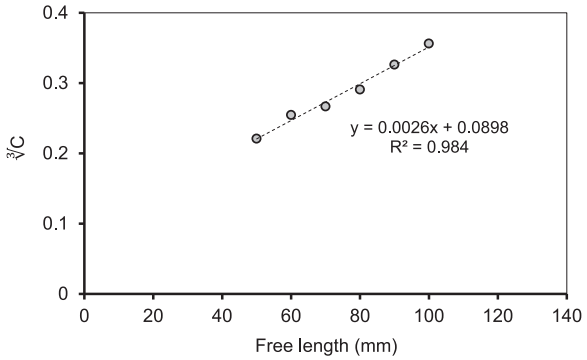

Fig. 7. A typical compliance calibration graph.

$$a_e = [\frac{1}{3}(2bCh^3E_1 - (L + \Delta_{clamp})^3]^{\frac{1}{3}} \tag{4}$$

This effective crack length is then used to calculate G_{IIC} using Equation (5).

$$G_{IIC} = \frac{9P^2{a_e}^2}{4b^2h^3E_1} \tag{5}$$

3. Results and analysis

3.1. DCB test results

Five DCB tests were conducted following the method in Section 2.2.

The force versus displacement curve is provided for all five tests, as illustrated in Fig. 8. The stiffness of the specimens varies slightly, due to the variability in flexural modulus between different DCB specimens.

R-curve for each specimen is illustrated in Fig. 9.

The load at which the crack starts to initiate from the film insert is used to calculate the Mode I fracture energy initiation value. The peak load is used to calculate the maximum Mode I fracture energy value. The initial points, $G_{IC,\ initiation}$ and maximum points, $G_{IC,\ \max}$ are also listed in Table 1.

The significant upward trend noted in the Mode I R-curves (Fig. 9) is mainly due to fibre bridging, a phenomenon that is further intensified by the random characteristics of the CF-SMC architecture. In contrast to continuous or unidirectional composites, CF-SMC comprises randomly orientated discontinuous fibre strands. As the crack propagates from the initial film end, it promotes clusters of already broken fibres to be pulled away along the main fracture plane, namely fibre bridging, leading to increased fracture resistance. Sometimes even the entire tapes are pulled away (Fig. 3). The spatial variability of fibre orientation induces localised areas of increased fracture resistance, leading to a stepwise or nonlinear enhancement in fracture energy (Fig. 9). The random fibre orientation distribution and resin-rich zones also result in large variability in R-curves, which is absent in continuous fibre composite laminates.

There is a significant increase of 572 % on average in Mode I fracture energy values from the average initiation value to the maximum value. This is because of fibre bridging in CF-SMC specimens as seen in Fig. 3.

3.2. ELS test results

Four ELS specimens were pre-cracked according to the ISO 15114 standard. They were tested following the method in Section 2.3.

Force vs. displacement curves are plotted in Fig. 10. There is a load drop in ELS Test 1 early on which is likely due to slippage inside the grip. During data reduction, its load–displacement curve is shifted so the linear portion later is aligned with the origin. The stiffness of the specimens varies significantly, potentially due to the variability in crack lengths, flexural moduli and internal morphology including fibre waviness between different ELS specimens. ELS Test 4 also has its bonded hinge turned around, so the film end is further away from the hinge pin centre than the rest of the specimens. This was done to create a longer film insert length to stabilise the crack propagation.

The fracture energy values were calculated, and consequent R-curve was plotted for each specimen as shown in Fig. 11.

The initiation values of Mode II fracture energy are based on 5 % change of compliance according to the ISO 15114 standard [17]. The peak loads were used to calculate the maximum value of Mode II fracture energy. The R-curves end when unstable fracture occurs, and sometimes the crack reaches the clamp. The initiation values, $G_{IIC,\ initiation}$, and maximum values, $G_{IIC,\ \max}$, are listed in Table 2.

R-curves were observed in some ELS tests. Considering the large variability in initiation values for G_{IIC}, there is no clear trend for the enhancement of G_{IIC} during fracture propagation. After examining the images of failed ELS specimen under loads, it was found that the crack propagates from the film end (the first vertical mark on the white paint) and sometimes migrates into the different layers of ELS specimens as shown in Fig. 12. Crack migration did not appear in ELS Test 1 (Fig. 12a). but showed in other ELS tests leaving traces

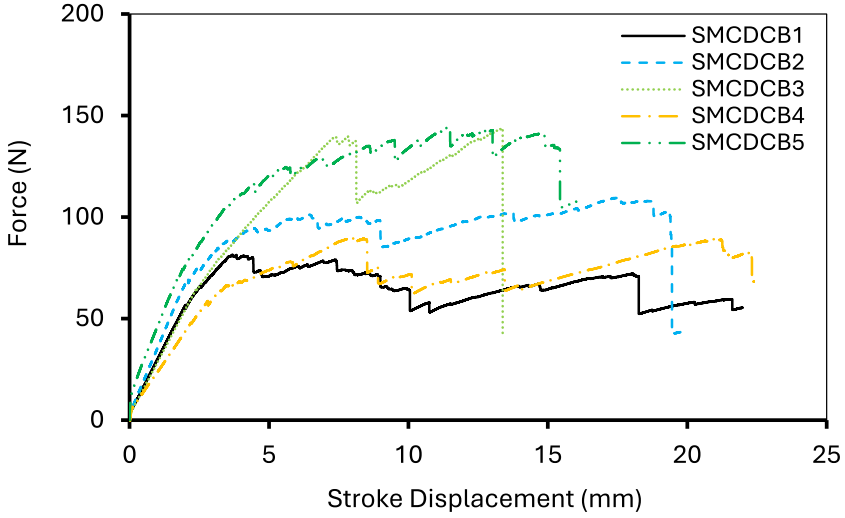

Fig. 8. Force vs. displacement curves from the DCB tests.

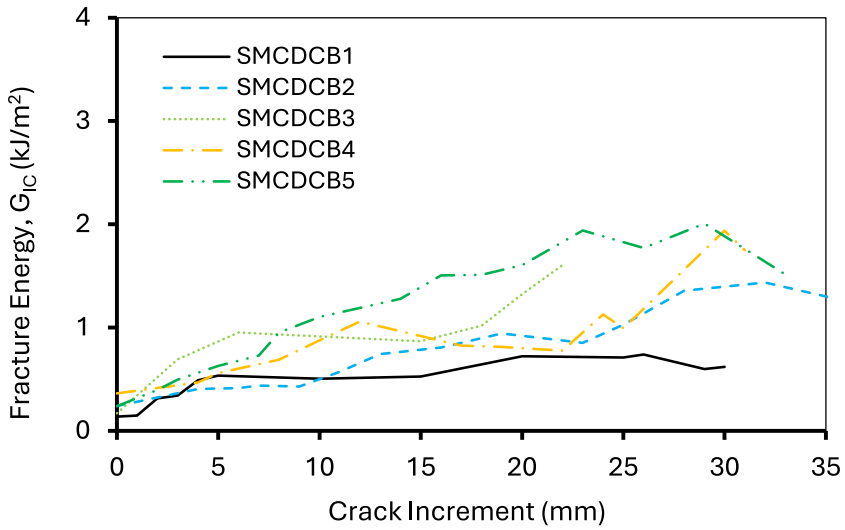

Fig. 9. R-curves from the DCB tests.

Table 1
Mode I fracture energy for each specimen and average.

Specimen	$G_{IC,\ initiation}$ [kJ/m^2]	$G_{IC,\ max}$ [kJ/m^2]
SMCDCB1	0.14	0.74
SMCDCB2	0.24	1.44
SMCDCB3	0.17	1.61
SMCDCB4	0.36	1.94
SMCDCB5	0.24	2.01
Average	0.23	1.55
C.V.	37.6 %	32.9 %

of detached fibre strands. Specifically, crack migration happened later in ELS Test 2 (Fig. 12b) and early on in ELS Test 4 (Fig. 12d). Crack migration occurred at multiple locations throughout ELS Test 3 (Fig. 12c). The fracture sequences match the change in R-curves well, each followed by an enhancement of fracture resistance as shown in Fig. 12. This proves that the toughening mechanism under Mode II is crack migration between different tape layers.

The substantial coefficient of variation (49.3 %) in Mode II initiation values mainly arises from variability in fibre orientation at the

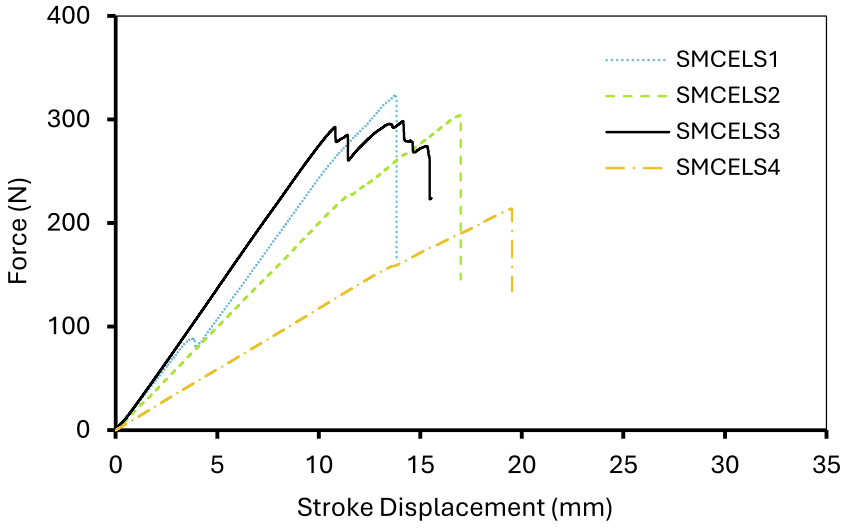

Fig. 10. Force vs. displacement curves from the ELS tests.

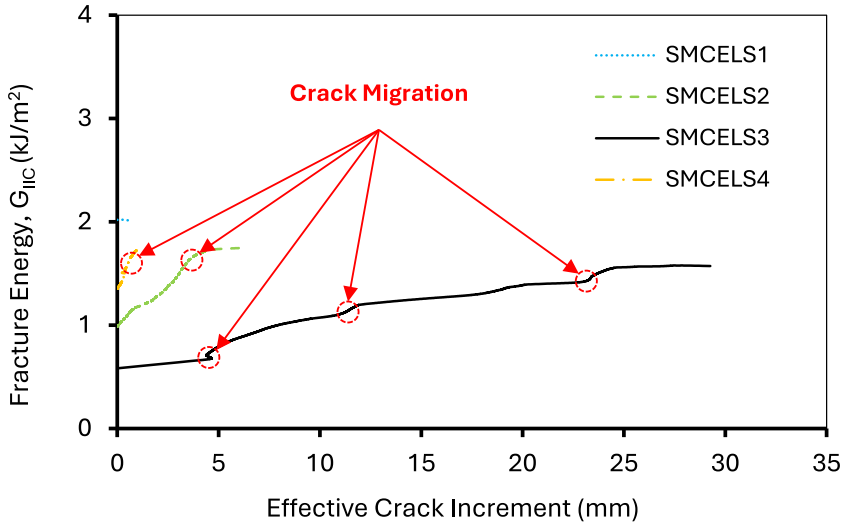

Fig. 11. R-curves from the ELS tests.

Table 2
Mode II fracture energy for each specimen and average.

Specimen	$G_{IIC,\ initiation}$ [kJ/m^2]	$G_{IIC,\ max}$ [kJ/m^2]
SMCELS1	2.02	2.02
SMCELS2	0.99	1.75
SMCELS3	0.58	1.58
SMCELS4	1.35	1.73
Average	1.24	1.77
(C.V.)	49.3 %	10.4 %

pre-crack tip among specimens. This results in variable crack migration locations from specimen to specimen due to different local fibre orientations. An earlier crack migration would lead to higher initiation value. This diversity illustrates the stochastic morphology of CF-SMC; nevertheless, establishing a quantifiable relationship with fibre orientation necessitates further microstructural investigation, which is beyond the scope of this study.

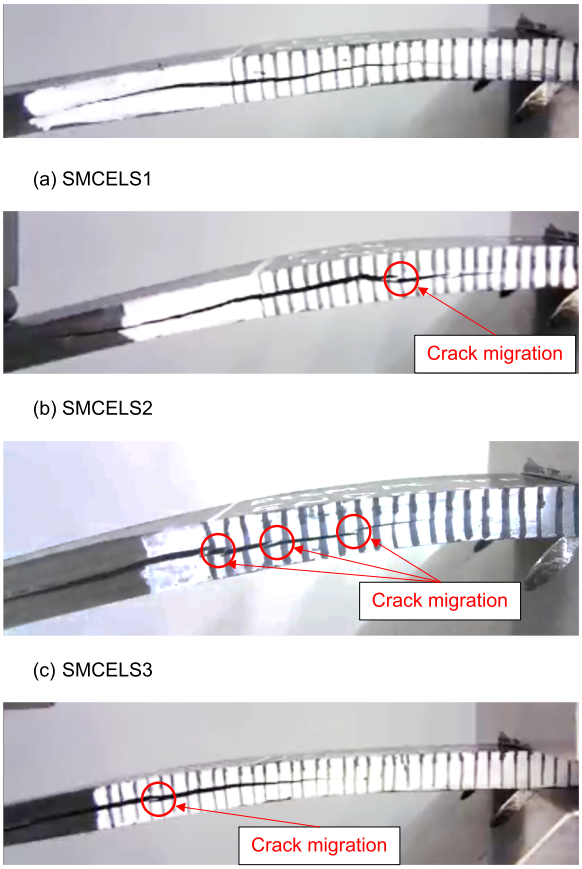

Fig. 12. Crack migrations in the ELS tests.

4. Discussion

Tiefenthaler et al. [15] reported single G_{IC} (1.83 kJ/m^2, C.V. 29.6 %) and G_{IIC} (3.13 kJ/m^2, C.V. 17.6 %) values for the same HexMC material using DCB and ENF test methods. These values are comparable to maximum G_{IC} (1.55 kJ/m^2, C.V. 32.9 %) and G_{IIC} (1.77 kJ/m^2, C.V. 10.4 %) from this work, considering the large variability in CF-SMC materials. However, they did not report any R-curves or provide any evidence for the toughing mechanisms, only stating crack stopping behaviour due to the random distribution of the tapes.

Further initiation values from this work confirmed the R-curve behaviour and provide new insight into fracture resistance in CF-SMC materials. The evidence of fibre bridging and crack migration supports the observed R-curves in the current DCB and ELS tests, respectively. When modelling CF-SMC materials, the Mode I fracture resistance enhancement effects or R-curves cannot be ignored due to significant fibre bridging. The Mode II fracture energy is commonly seen as a constant value when modelling CF-SMC e.g. 1 kJ/m^2 [12,13]. The current study shows that R-curves were seen in some ELS tests when crack migration occurred between tape layers. This can potentially justify the usage of a relatively low Mode II fracture energy value if significant crack growth is not expected.

5. Conclusions

DCB and ELS tests were conducted on a CF-SMC material to understand its Mode I and Mode II fracture resistance, respectively. A significant Mode I R-curve was observed for the HexMC material tested, showing a 572 % increase in average fracture energy due to fibre bridging. For Mode II, R-curves were observed in some tests due to crack migration between tape layers, but the average trend is not conclusive due to a large variation in initiation values. In both Mode I and Mode II fracture tests, the fracture energy values show a large scatter from specimen to specimen. The maximum fracture energy values ($G_{IC,\ \max} = 1.55$ kJ/m^2, $G_{IIC,\ \max} = 1.77$ kJ/m^2) are comparable to those reported in the literature for the same HexMC material. The R-curves including the new initiation values ($G_{IC,\ initiation} = 0.23$ kJ/m^2, $G_{IIC,\ initiation} = 1.24$ kJ/m^2) measured in the current experiments provide critical inputs for failure analyses of CF-SMC materials.

CRediT authorship contribution statement

Xiaodong Xu: Writing – review & editing, Validation, Supervision, Project administration, Methodology, Investigation, Conceptualization. **Darren Kong Kiat Lo:** Writing – original draft, Visualization, Investigation, Formal analysis, Data curation. **Ilham Akbar Adi Satriya:** Writing – original draft, Visualization, Investigation, Data curation. **Liyi Zheng:** Writing – review & editing.

Declaration of competing interest

The authors declare that they have no known competing financial interests or personal relationships that could have appeared to influence the work reported in this paper.

Acknowledgements

The authors would like to thank Professor Michael R. Wisnom from the Bristol Composites Institute of the University of Bristol for his valuable feedback on the paper.

The authors thank Dr David Ayre and Mr Jim Hurley from the Composites and Advanced Materials Centre at Cranfield University for their advice on processing the HexMC material.

Data availability

Data will be made available on request.

References

[1] Barbero EJ. Introduction to Composite Materials Design. Third Edition. Boca Raton: CRC Press - Taylor & Francis Group; 2018.
[2] Fortune Business Insights. Carbon Fibre Market Size, Share & Industry Analysis, By Precursor (PAN and Pitch), By Tow (Large Tow and Small Tow), By Application (Aviation, Aerospace & Defense, Automotive, Wind Turbines, Sports & Leisure, Construction, and Others), and Regional Forecast, 2024-2032. accessed July 15, 2024 Adv Mater 2024. https://www.fortunebusinessinsights.com/industry-reports/carbon-fiber-market-101719.
[3] Ishikawa T, Amaoka K, Masubuchi Y, Yamamoto T, Yamanaka A, Arai M, et al. Overview of automotive structural composites technology developments in Japan. Compos Sci Technol 2018;155:221–46. https://doi.org/10.1016/j.compscitech.2017.09.015.
[4] United Nations. Sustainable Development Goals (SDGs). Sustainable Development Goals (SDGs) 2023. https://sdgs.un.org/ (accessed July 15, 2024).
[5] Zhang J, Chevali VS, Wang H, Wang CH. Current status of carbon fibre and carbon fibre composites recycling. Compos B Eng 2020;193. https://doi.org/10.1016/j.compositesb.2020.108053.
[6] Almushaikeh AM, Alaswad SO, Alsuhybani MS, AlOtaibi BM, Alarifi IM, Alqahtani NB, et al. Manufacturing of carbon fiber reinforced thermoplastics and its recovery of carbon fiber: A review. Polym Test 2023;122. https://doi.org/10.1016/j.polymertesting.2023.108029.
[7] Yildirim C, Ulus H, Beylergil B, Al-Nadhari A, Topal S, Yildiz M. Tailoring adherend surfaces for enhanced bonding in CF/PEKK composites: Comparative analysis of atmospheric plasma activation and conventional treatments. Compos Part A Appl Sci Manuf 2024;180:108101. https://doi.org/10.1016/j.compositesa.2024.108101.
[8] Topal S, Al-Nadhari A, Yildirim C, Beylergil B, Kan C, Unal S, et al. Multiscale nano-integration in the scarf-bonded patches for enhancing the performance of the repaired secondary load-bearing aircraft composite structures. Carbon N Y 2023;204:112–25. https://doi.org/10.1016/j.carbon.2022.12.056.
[9] Zhao Z, Wan Y, Xu X, Takahashi J. Influence of one-dimensional material flow on mechanical properties and fiber orientation distribution of thin-ply carbon fiber reinforced thermoplastics sheet molding compounds. Compos Commun 2024;51. https://doi.org/10.1016/j.coco.2024.102071.
[10] Satriya IAA, Kadir AM. Numerical Computations and Experimental Tests on High Aspect Ratio Composite Wing Structure Due to Static Load. AIP Conf Proc, vol. 2941, 2023. doi: 10.1063/5.0181433.
[11] ASTM International. D7905/D7905M : Standard Test Method for Determination of the Mode II Interlaminar Fracture Toughness of Unidirectional Fiber-Reinforced Polymer Matrix Composites 2015. doi: 10.1520/D7905_D7905M-14.
[12] Kravchenko SG, Sommer DE, Denos BR, Favaloro AJ, Tow CM, Avery WB, et al. Tensile properties of a stochastic prepreg platelet molded composite. Compos Part A Appl Sci Manuf 2019;124. https://doi.org/10.1016/j.compositesa.2019.105507.
[13] Li Y, Pimenta S, Singgih J, Nothdurfter S, Schuffenhauer K. Experimental investigation of randomly-oriented tow-based discontinuous composites and their equivalent laminates. Compos Part A Appl Sci Manuf 2017;102:64–75. https://doi.org/10.1016/j.compositesa.2017.06.031.
[14] Taketa I, Okabe T, Kitano A. A new compression-molding approach using unidirectionally arrayed chopped strands. Compos Part A Appl Sci Manuf 2008;39:1884–90. https://doi.org/10.1016/j.compositesa.2008.09.012.
[15] Tiefenthaler M, Stelzer PS, Chung CN, Reisecker V, Major Z. In: Characterization of the fracture mechanical behavior of C-SMC materials. Czech Technical University in Prague; 2018. p. 1–5. https://doi.org/10.14311/APP.2018.18.0001.
[16] ASTM International. D5528/D5528M − 21 − Standard Test Method for Mode I Interlaminar Fracture Toughness of Unidirectional Fiber-Reinforced Polymer Matrix Composites 2021. doi: 10.1520/D5528_D5528M-21.
[17] International Standard. ISO 15114 - Fibre-reinforced plastic composites — Determination of the mode II fracture resistance for unidirectionally reinforced materials using the calibrated end-loaded split (C-ELS) test and an effective crack length approach. 2014.

https://dspace.org/

An experimental investigation into fracture resistance of carbon fibre sheet moulding compound

Xu, Xiaodong; Kiat Lo, Darren Kong; Adi Satriya, Ilham Akbar; Zheng, Liyi

2025-06-26
Elsevier
https://doi.org/10.1016/j.engfracmech.2025.111198
Xu X, Kiat Lo DK, Adi Satriya IA, Zheng L. (2025) An experimental investigation into fracture resistance of carbon fibre sheet moulding compound. Engineering Fracture Mechanics, Volume 323, June 2025, Article number 111198

Downloaded from a DSpace repository. https://dspace.org/